STRONG MOTIONS FROM A STOCHASTIC MODEL OF FAULTING

Y. SUZUKI (I)
T. HIRASAWA (II)
Presenting Author : Y. SUZUKI

SUMMARY

We propose a faulting model valid for a wide frequency range of seismic waves. High frequency waves are considered to be generated by inhomogeneous distribution of strength on the fault plane, which is divided into many small sub-areas. The size of sub-area, local stress drop, and rupture velocity are treated as random variables. We discuss the characteristics of acceleration source spectra expected for the model. Finally we apply our model to the Miyagi-Oki, Japan, earthquake of 1978 and to the Japan Sea earthquake of 1983 to synthesize theoretical accelerograms.

INTRODUCTION

It is well recognized among seismologists that high frequency strong seismic motions cannot be explained by simple deterministic fault models. Many investigators have considered more generalized fault or crack models so as to efficiently generate high frequency waves. About these investigations, the extensive reviews by Aki (Ref. 1) and by Boore (Ref. 2) should be referred to. We restrict ourselves to the direct predecessors of the stochastic model presented here.

Hirasawa et al. (Refs. 3 and 4) proposed a simple stochastic fault model in which the fault was composed of small sub-areas. Stress drops of sub-areas were assumed not to be constant over the whole fault, but to be random. They derived an analytical expression for power spectral amplitude of acceleration, using the expression given by Sato and Hirasawa (Ref. 5) for the far-field waveform from a circular crack, and assuming that the acceleration waves can be regarded as a stochastic shot noise process. The amplitude of high frequency components was found to be proportional to $\sqrt{E(\tau^2)}$, the root mean square of local stress drop τ. They also found that the peak acceleration approaches to a limiting value when L/r becomes larger than about 2, where L is the fault radius and the closest distance r from the fault to an observation point is fixed to a finite value.

The amplitude of low frequency components is proportional to global stress drop $\Delta\sigma$. Although the global stress drop is considered, to a first approximation, to be identical to $E(\tau)$, the mean value of τ, it is not necessarily equal to $E(\tau)$. Anyway we now have two quantities of $\Delta\sigma$ or $E(\tau)$ and $E(\tau^2)$ which characterize excitations of low and high frequency components of seismic waves. Izutani (Ref. 6) has proposed a method to predict near-field acceleration waveforms utilizing the above simple stochastic model, to obtain the ratio of the root mean square of local stress drop to

(I) Research Associate, Fac. of Sci., University of Tokyo, Tokyo, Japan

(II) Professor, Fac. of Sci., Tohoku University, Sendai, Japan

global stress drop.

In the present study we present a stochastic model of faulting in which we include the gross effect of macroscopic rupture propagation on radiated seismic waves.

DESCRIPTION OF THE STOCHASTIC MODEL

Our model is shematically illustrated in Fig.1. The fault plane with length L and width W is divided into many sub-areas. The gross rupture is initiated at a point on the fault plane, as indicated by the big star symbol in the upper left of Fig.1. In a macroscopic scale, rupture spreads radially with an average rupture velocity v, and the rupture front in an average sense is shown by a broken line in the upper left of Fig.1. Now the sub-area may have any shape; here we adopt the square sub-area for the sake of simplicity. The rupture within an sub-area is shown in the lower left of Fig.1; the rupture nucleates at the center and spreads the sub-area bidirectionally. The source time function adopted here is the unit step function. The random variables are local stress drop τ, rupture velocity v, the rotation angle γ of the sub-area with respect to the strike direction of the fault, as shown in the lower left of Fig.1, and the size a of the sub-area. These variables except for the local stress drop and the size are assumed to be uniformly distributed in finite intervals. The probability density function of τ is discussed in the next section, and that of size a is assumed to be inversely proportional to the square root of the size.

The far field waveforms from a quarter A of a sub-area is illustrated in the right part of Fig.1. The magnitude of the short-period acceleration pulse is proportional to the local stress drop. Though contribution of this acceleration pulse to the high frequency energy of the resultant waves would be sufficient, that of the seismic moment is too small for the fault with length L and width W. To compensate the defficiency of the seismic moment, we introduced the long-period pulse as illustrated in the upper right of Fig.1. The rise time of the displacement waveform of this long-period pulse is assumed to be $2a/v$, and the amplitude of this displacement waveform is determined so that the sum of seismic moment of the short-period pulse and that of the lomg-period pulse is equal to the seismic moment expected deterministically for the fault. The acceleration waveform for our stochastic model is expressed as the sum of short- and long-period pulses emitted from all sub-areas.

CHARACTERISTICS OF SOURCE SPECTRA

To discuss the characteristics of seismic source spectra expected for our model, we adopt a particular fault geometry in which fault length and width are taken as 80 km and 30 km, respectively. This fault geometry is the case for Miyagi-Oki earthquake of 1978 with a magnitude of 7.4. The coordinate system used is illustrated in Fig. 2. The rupture is initiated at $(x = -L/2, y = 0)$ in unilateral cases and at $(x = 0, y = 0)$ in the bilateral cases. The hypocentral distance of a station S is taken to be 1000 km. When no explanatory note is given, an average size $(2\overline{\Delta L})$ of sub-areas is 2 km and a bimodal distribution with $\sqrt{E(\tau^2)}/E(\tau) = 2.0$, as illustrated in Fig. 3, is assumed for the probability density function of local stress drop. As stated before, the propagation direction of bidirectional ruptures in sub-areas are assumed to be random.

Fig 4 shows examples of average source spectra in acceleration of P and

S waves computed for a station of $\theta = 60^\circ$ and $\phi = 180^\circ$ in the case of unilateral faulting. This average spectrum is obtained from ten samples of spectral densities computed by using different sets of random number. The dash lines approximate the average spectra shown by the solid curves. There exist three corner frequencies of f_L, f_I, and f_H as denoted in the simplified spectra, and the spectral density is proportional to f^2 for $f < f_L$ and to f for $f_I < f < f_H$. The lower corner frequency f_L is identical to the conventional corner frequency in a deterministic fault model. A similar source spectrum in acceleration has been introduced semi-empirically by Izutani (Ref. 6).

Fig. 5 illustrates the effects of $E(\tau^2)$ and $\overline{\Delta\tau}$ on the source spectra, where ST = 2.0 corresponds to the bimodal distribution and ST = 1.15 does to the uniform distribution of local stress drop as shown in Fig. 3. We observe from this that the amplitude at frequencies higher than f_H depends not on $\overline{\Delta\tau}$ but on $E(\tau^2)$, and that f_H is approximately in inverse proportion to $\overline{\Delta\tau}$. Fig. 6 exhibits the directivity of acceleration spectra obtained for unilateral and bilateral faultings. The directivity at higher frequencies is much stronger in S waves than in P waves. Our stochastic model predicts also that f_H for P waves is not higher than that for S waves. It is concluded that the macroscopic or average motion of faulting governs the source spectra for $f < f_I$, the microscopic or random motion of faulting does those for $f > f_H$, and the spectra for $f_I < f < f_H$ can be regarded as transitional ones.

SYNTHESIZED ACCELEROGRAMS

To simulate the acceleration waveforms at an observation point on the earth's surface, we took into accounts the radiation pattern in S wave amplitude due to the focal mechanism, the effect of inelastic attenuation through the propagation path, and the response of the velocity structure beneath the observation site. The velocity structure used for computation are listed in Table 1.

Miyagi-Oki earthquake of 1978

This earthquake took place off the coast of the Miyagi Prefecture, northeastern Japan on June 12, 1978. Its epicenter,depth, and magnitude determined by JMA(Japan Meteorological Agency) are 38°09'N, 142°10'E, 40 km, and 7.4, respectively. Seno et al.(Ref. 7) investigated the rupture process to obtain three fault models called 1-, 2-, and 3-segment models, among which 1- and 3-segment models are listed in Table 2. The 1-segment model was derived from observed long-period seismic waves, while the 3-segment model was introduced to satisfy shorter period components of body waves.

First we calculate the acceleration waveforms at Ofunato, which is situated at about 100 km north-northwest of the epicenter and about 90 km northeast of Sendai. Fig. 7 shows the observed accelerograms at Ofunato. The simulated accelerograms are presented in Fig. 8 in the case of 1-segment model, in which the bimodal distribution of local stress drop is assumed. Fig. 9 shows the accelerograms computed for 3-segment model. In this case, local stress drop is assumed to be uniformly distributed in each segment. The agreement between the theoretical peak accelerations and the observed ones are satisfactory in horizontal components.

Next we carried out a similar simulation for Sendai, which is located at about 120 km west of the epicenter. Fig. 10 is an example of the observed accelerograms at Sendai. The velocity structure listed in Table 1 is that for Katahira town in Sendai city. The agreement of the theoretical accel-

erograms, Figs. 11 and 12 for 1- and 3-segment models respectively, with the observed ones is worse than that for Ofunato.

Japan Sea earthquake of 1983

This earthquake occurred on May 26, 1983. Its epicenter, depth, and magnitude determined by JMA are 41°21'N, 139°05'E, 14 km, and 7.7. Fig. 13 shows the aftershock distributions determined by Tohoku University, where the main shock is indicated by the open star in the left figure and the largest aftershock(June 21, M = 7.1) by the open star in the middle. Fig. 14 illustrates 1- and 2-segment fault models based on those by Shimazaki and Mori(Ref. 8) and Mori and Shimazaki(Ref. 9), where the main shock and the largest aftershock are designated by M and A, respectively. The accelerograms of the main shock at Hirosaki by Hirosaki University are given in Fig. 15. Since the ground structure at Hirosaki is not well known, we used the velocity model of Katahira listed in Table 1. Figs. 16 and 17 show the simulated accelerograms at Hirosaki for 1- and 2-segment models, respectively.

DISSCUSSIONS

In our model the dislocation time function was assumed to be a step function in each sub-area, as described before. It comes from this assumption that the acceleration spectra are flat at frequencies higher than f_H. The cut-off frequency, f_{max}, beyond which the acceleration spectrum decays, is often found in the observed acceleration spectra. Whether the observed f_{max} resulted from the source characteristics or from the site effect is still in question(Refs. 10 and 11). However, if we introduce a sufficiently small rise time to the dislocation time function in sub-areas, f_{max} will appear at a frequency higher than f_H, and spectral amplitude exhibits f^{-1} decay for $f > f_{max}$. In this case the same value of f_{max} is expected for both P and S waves.

A simple scaling relation can be derived for the source spectra from our model, provided that the following similarity condition holds: The probability density functions are unchanged for such random variables as local stress drop, rupture velocity, etc. and L/r, W/L, and $\Delta L/L$ are constant. Let us denote the time function of acceleration in the case of fault length L_0 as $a_0(t)$ and its Fourier transform as $A_0(\omega)$. The acceleration $a(t)$ or $A(\omega)$ in the case of $L = \alpha L$ at a distance of αr is expressed by $a_0(t/\alpha)/\alpha$ or $A(\alpha\omega)$, α being a positive constant.

Our simulation of accelerograms are not satisfactory except for the relatively hard rock site of Ofunato. The most significant disagreement between the theory and the observation is seen in the amplitude ratio of two horizontal components. The directivity due to the radiation pattern is quite effective to the theoretical accelerograms, while the observed ones seem to be more isotropic. In calculating the radiation pattern terms we used a representative take-off angle of the seismic ray from a sub-area. It is possible to expect that the seismic rays in a considerable range of take-off angles arrive at a station to weaken the directivity due to radiation pattern terms.

REFERENCES

1. Aki, K., Strong motion prediction using mathematical modeling techniques, *Bull. Seism. Soc. Am.*, 72, S1-S13, 1982.

2. Boore, D. M., Strong-motion seismology, *Rev. Geophys. Space Phys.*, 21, 1308-1318, 1983.
3. Hirasawa, T. and K. Yamamoto, Prediction of peak acceleration from a stochastic source model, (in Japanese), *Abstracts Seism. Soc. Japan*, 1977, No. 2,p. 142,1977.
4. Hirasawa, T., J. Oda, and K. Yamamoto, Miyagi-Ken-Oki earthquake and peak acceleration, (in Japanese), *Proc. 17 Symp. Natural Disaster Sci.*, 515-516, 1980.
5. Sato, T. and T. Hirasawa, Body wave spectra from propagating shear cracks, *Jour. Phys. Earth*, 21, 415-431, 1973.
6. Izutani, Y., A statistical model for prediction of quasi-realistic strong motion, *Jour. Phys. Earth*, 29, 537-557, 1981.
7. Seno, T., K. Shimazaki, P. Sommerville, K. Sudo, and T. Eguchi, Rupture process of the Miyagi-Oki, Japan, earthquake of June 12, 1978, *Phys. Earth Planet. Int.*, 23, 39-61, 1980.
8. Shimazaki, K. and J. Mori, Focal mechanism of the May 26, 1983 Japan Sea earthquake, *Abstracts Seism. Soc. Japan*, 1983, No. 2, p. 15, 1983.
9. Mori, J. and K. Shimazaki, Source process of the May 26, 1983 Japan Sea earthquake, *Abstracts Seism. Soc. Japan*, 1983, No. 2, p. 16, 1983.
10. Hanks, T. C., f_{max}, *Bull. Seism. Soc. Am.*, 72, 1867-1879, 1982.
11. Papageorgiou, A. S. and K. Aki, A specific barrier model for the quantitative description of inhomogeneous faulting and the prediction of strong ground motion. Part II Applications of the model, *Bull. Seism. Soc. Am.*, 73, 953-978, 1983.

Table 1. Ground structures

	thickness (m)	S vel. (km/s)	density (g/cm^3)	Q_S
Ofunato	360 —	1.5 2.5	2.3 2.5	100 —
Katahira	8 192 200 —	0.23 0.61 1.5 3.0	1.7 2.0 2.3 2.5	15 30 100 —

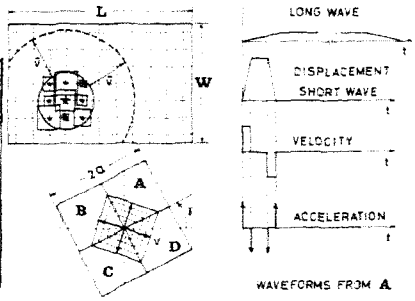

Fig. 1. Stochastic model

Table 2. Fault parameters

	1-seg. model	3-seg. model 1st	2nd	3rd
length (km)	80	10	27	24
width (km)	30	17	34	34
moment	3.1	0.5	1.3	1.3
slip (m)	1.8	4.2	2.0	2.3
stress drop (bar)	70	550	110	135

moment is given in 1×10^{27}dyne·cm

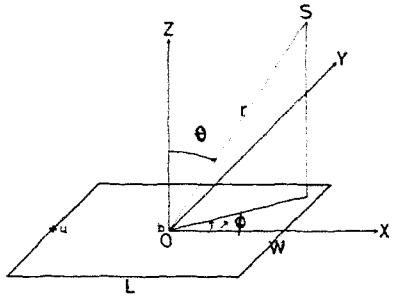

Fig. 2. Coordinate system.

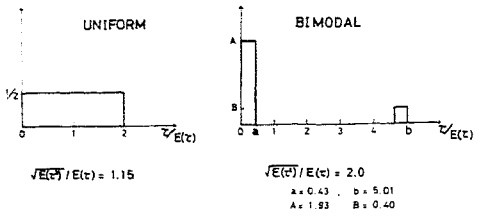

Fig. 3. Two kinds of probability density function considered.

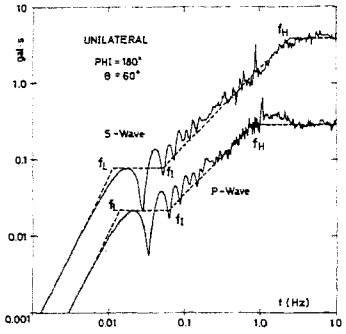

Fig. 4. Averaged acceleration source spectra.

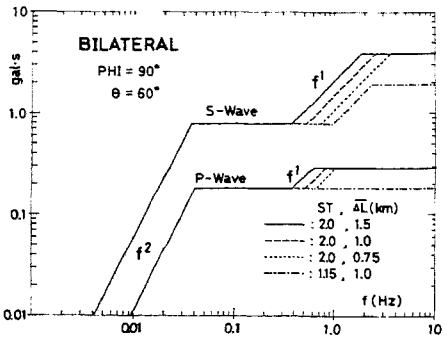

Fig. 5. Effects of $E(\tau^2)$ and ΔL(mean of a) on acceleration source spectra.

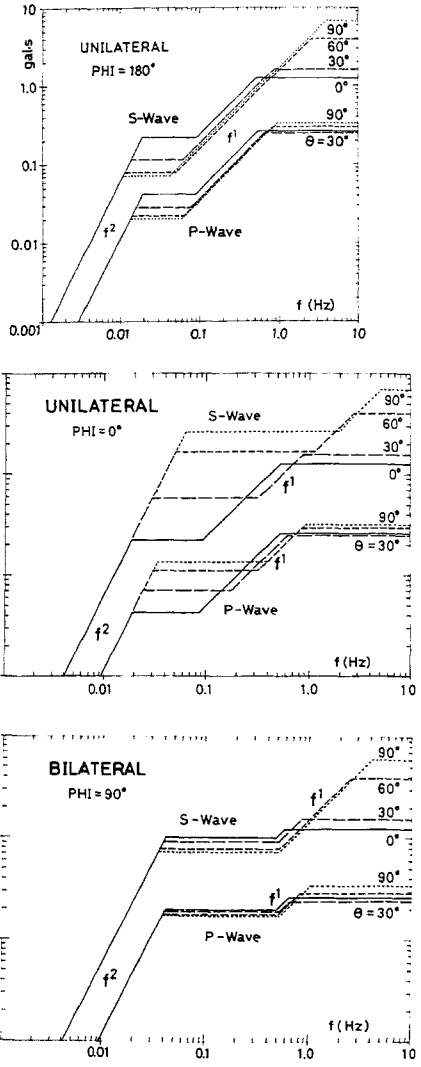

Fig. 6. Directivity of acceleration spectra as function of θ.

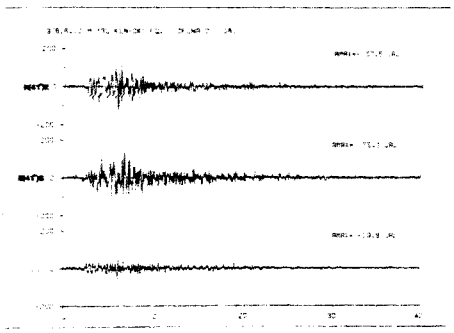

Fig. 7. Accelerograms observed at Ofunato.

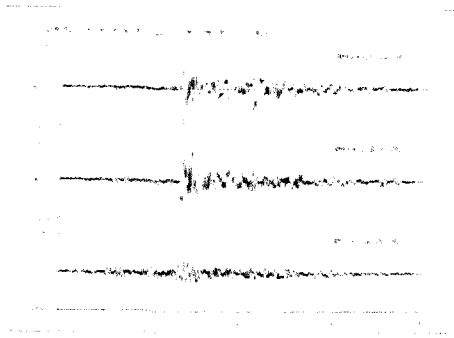

Fig. 10. An example of accelerograms observed at Sendai.

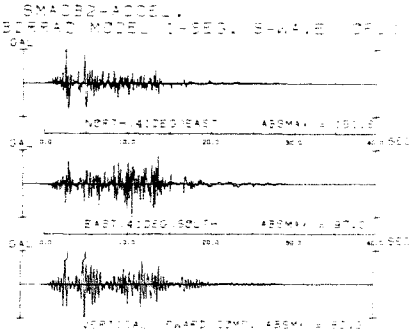

Fig. 8. Computed accelerograms for 1-segment model. (Ofunato)

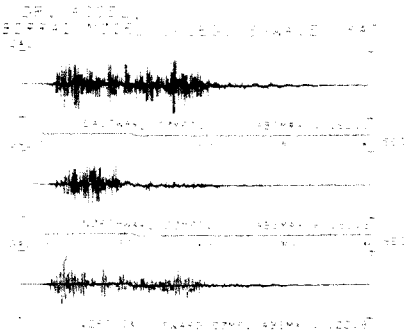

Fig. 11. Computed accelerograms for 1-segment model. (Katahira,Sendai)

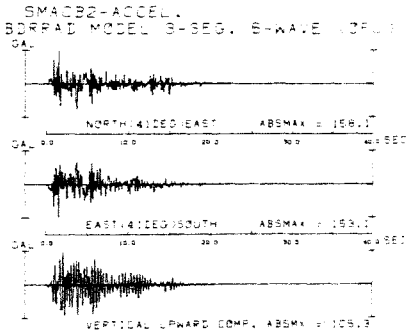

Fig. 9. Computed accelerograms for 3-segment model. (Ofunato)

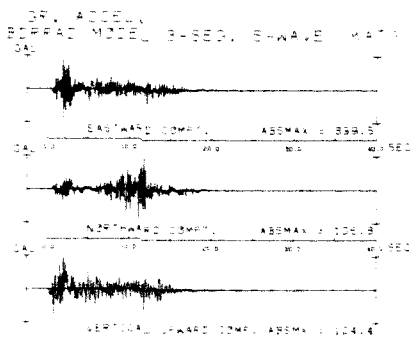

Fig. 12. Computed accelerograms for 3-segment model. (Katahira)

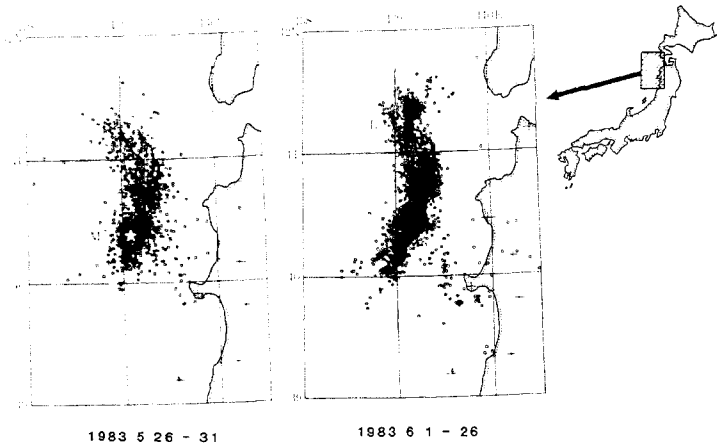

Fig. 13. Aftershock distribution during two intervals: May 26-31,left and June 1-26,right.

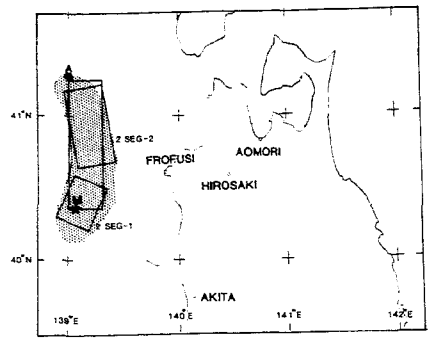

Fig. 14. 1- and 2-- segment models.

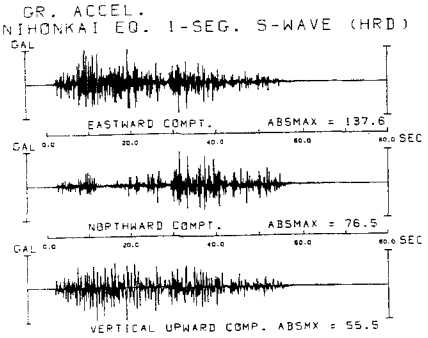

Fig. 16. Synthesized accelerograms at Hirosaki for 1-segment model.

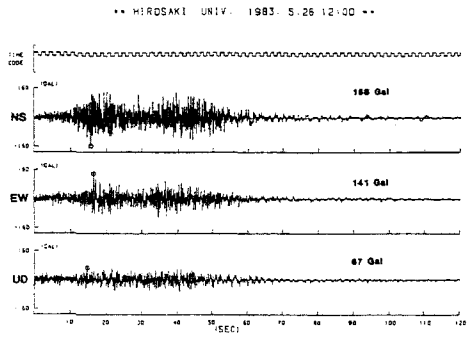

Fig. 15. Accelerogram observed at Hirosaki.

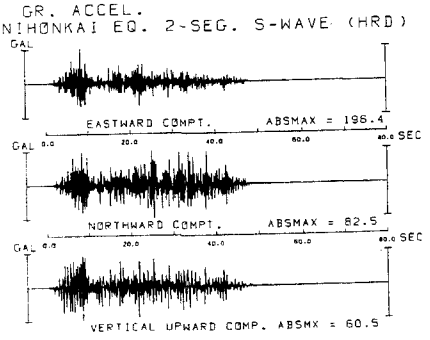

Fig. 17. Synthesized accelerograms for 2-segment model.